Geomechanics and Engineering, *Vol. 16, No. 5 (2018) 495-501*
DOI: https://doi.org/10.12989/gae.2018.16.5.495

Discrete element modelling of geogrids with square and triangular apertures

Cheng Chen[1a], Glenn McDowell[2b] and Rui Rui*[1]

[1]School of Civil Engineering and Architecture, Wuhan University of Technology, Wuhan, 430070 China
[2]Nottingham Center for Geomechanics, University of Nottingham, Nottingham, U.K.

(Received May 22, 2018, Revised July 24, 2018, Accepted September 13, 2018)

Abstract. Geogrid application that has proved to be an effective and economic method of reinforcing particles, is widely used in geotechnical engineering. The discrete element method (DEM) has been used to investigate the micro mechanics of the geogrid deformation and also the interlocking mechanism that cannot be easily studies in laboratory tests. Two types of realistically shaped geogrid models with square and triangle apertures were developed using parallel bonds in PFC3D. The calibration test simulations have demonstrated that the precisely shaped triangular geogrid model is also able to reproduce the deformation and strength characteristics of geogrids. Moreover, the square and triangular geogrid models were also used in DEM pull-out test simulations with idealized shape particle models for validation. The simulation results have been shown to provide good predictions of pullout force as a function of displacement especially for the initial 30 mm displacement. For the granular material of size 40 mm, both the experimental and DEM results demonstrate that the triangular geogrid of size 75 mm outperforms the square geogrid of size 65 mm. Besides, the simulations have given valuable insight into the interaction between particle and geogrid and also revealed similar deformation behavior of geogrids during pullout. Therefore, the DEM provides a tool which enable to model other possible prototype geogrid and investigate their performance before manufacture.

Keywords: DEM, geogrid; aperture shape; deformation behavior; interlocking mechanism; pullout test

1. Introduction

In the past decades, geogrids have been used to stabilize the base and subgrade aggregate layers in transport engineering, reduce the amount of aggregate used, extend their service life, and reduce the construction cost (Koerner 2009). Soils pull apart under tension. Compared to soil, geogrids are strong in tension. This fact allows them to transfer forces to a larger area of soil than would otherwise be the case (Jenner 2009). Tensile strength of geogrid and the aggregate-geogrid interaction are the major factors which influence the improvement of the soil (Deb and Konai 2014). Change in the aperture of geogrid can change the interface behavior between aggregate and geogrid. The pullout resistance of the geogrid reinforcement is one of the most notable factors in increasing the bearing capacity of granular materials (Mahdi and Katebi 2015, Kim *et al*. 2018).

The discrete element method (DEM) (Cundall and Strack 1979), which has particular advantages in capturing the kinematic behavior of discontinuous martials at a microscopic level (McDowell *et al*. 2006, Bhandari and Han 2010, Chen *et al*. 2012), Previous researchers (Zhang *et al*. 2007, Wang *et al*. 2014) have demonstrated that pull-out test simulations in PFC2D using a geogrid consisting of a string of bonded particles. This 2D approach ignores the significant influence of the transverse ribs on the pullout resistance verified by the Mulabdic and Minazek (2010) on the basis of laboratory tests. Hence, it follows that only the 3-dimensional case is appropriate to simulate soil-geogrid interaction. Qian *et al*. (2013) and Tutumluer *et al*. (2010) used rigid wall elements to simulate the geogrid, while other focused on utilizing the parallel bond contact mode to bond different sphere arrangements and generate the required geogrid geometry (Konietzky *et al*. 2004, Han and Bhandari 2011, Ferellec and McDowell 2012, Chen *et al*. 2012, Ngo *et al*. 2014, Stahl *et al*. 2014). For the geogrid using wall elements, the geogrid doesn't have any deformation and gravity in PFC3D. Therefore, it should first be performed on the geogrid model to take into account its flexibility. It should also be noted that the more precise the numerical 3D geogrid model is, the longer the computational time will need.

Most of previous studies calibrated their geogrid models with the data obtained from the geogrid single rib test (ASTM D6637 2015). Other studies performed a more rigorous model calibration, including single junction test and In-plane rotation test. The majority of these studies performed DEM models of square geogrid, and a few of them modelled triangular geogrid (Chen *et al*. 2012, Ferellec and McDowell 2012). In this paper, two types of precisely shaped geogrid models with square and triangle apertures have been generated using parallel bonds, the micro parameters have then been calibrated by the single rib tensile test simulation. Afterwards, the pullout resistance and deformation behavior of geogrid models have been validated with experimental pullout test results.

*Corresponding author, Professor
E-mail: r.rui@whut.edu.cn
[a]Lecturer
E-mail: chengchen87@whut.edu.cn
[b]Professor

http://www.techno-press.org/?journal=gae&subpage=7
ISSN: 2005-307X (Print), 2092-6219 (Online)

2. Material and method

2.1 Polymer geogrid

Fig. 1 shows the tested polymer geogrid of with rectangular (65 × 65 mm) and triangular (65 × 75 × 75 mm) apertures, which are commonly used. The effective test areas of the square and triangular geogrids are almost the same for comparison. The components of the polymer square geogrid are also identified. The key feature of all geogrids is aperture which is the openings between the adjacent sets of longitudinal and transverse ribs. The shape and size of aperture should be large enough to allow for soil strike-through from one side of the geogrid to the other. In anchorage situations the soil strike-through within the apertures bears against the transverse ribs, which transmits the load to the longitudinal ribs via the junctions. The junctions (nodes) are, where the longitudinal and transverse ribs meet and are connected. The characteristics of square and triangular geogrids are listed in Table 1 (Tensar International 2010). In order to evaluate the effect of the aperture shape, both of the square and triangular geogrids have the same tensile stiffness and strength and also approximately the same area of coverage for a single reinforcing unit. The performance of biaxial and triaxial geogrids can be compared based on the pullout forces with the same effective geogrid area.

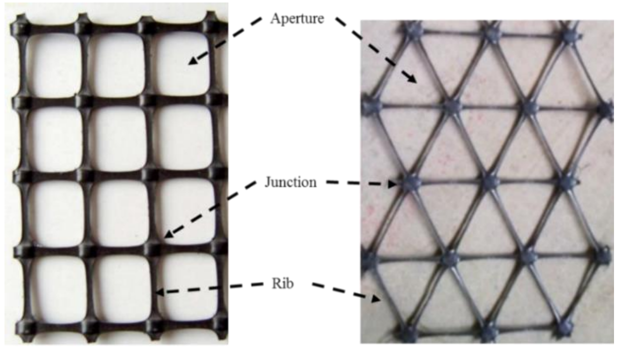

(a) (b)

Fig. 1 Geogrid samples: (a) square geogrid SSLA30 and (b) triangular geogrid TX130

Table 1 Geogrid sample characteristics

Geogrid Aperture	Square	Triangular
Rib length (mm)	65	75
Rib thickness (mm)	1.7	1.7
Rib width (mm)	4.0	4.0
Node thickness (mm)	7.0	7.0
Tensile strength (kN/m)	30	30
Coverage area of a reinforcing unit (m3)	0.17 (4 apertures)	0.15 (6 apertures)

2.2 Geogrid models of different aperture shapes

A parallel bond can be envisaged as a disc of elastic glue lying on the contact plane, as shown in Fig. 2. The parallel bond can transmit both forces and moments between particles, while contact bonds can only transmit forces acting at the contact point. Relative motion at the contact causes a force and a moment to develop within the parallel bond as a result of the stiffness of the parallel bond. The parallel bond breaks when the stress in any part of the bond exceeds the parallel bond strength (Itasca 2008).

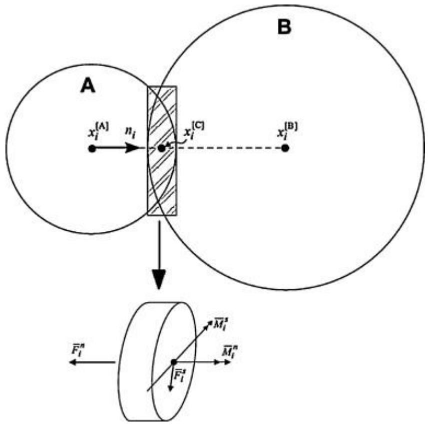

Fig. 2 Parallel bond Model

At the preliminary stage of this research, the single-ball chains were tried to use to model the square geogrid as shown in Fig. 3(a). To improve modelling of the square geogrid of aperture size 65 mm, the shape of the geogrid was reproduced by 168 single spheres of 3 mm radius bonded together by parallel bond. Fig. 3(b) shows the view of the single-ball triangular geogrid in form of the arranged particles and the parallel bonds between them, respectively. However, neither of them is considered a good geogrid model to reproduce the real geogrid behavior. The simulation results show the ribs of the single-sphere geogrid only deformed along the pullout direction, which cannot reveal the typical deflection behavior of real geogrid. The performance of two layers of spheres in a cross-section of rib would be better than a single layer of spheres and single row of spheres. Moreover, the different bending stiffness of geogrid rib along horizontal and vertical planes and a rectangular shaped cross-section of rib also would be considered. Therefore, a new two-layer geogrid model with a realistic shaped should be generated, and also the micro parameters need to be calibrated later.

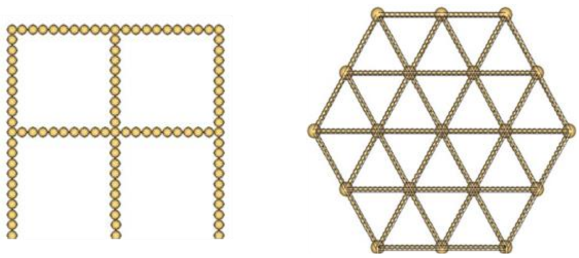

(a) Square geogrid (b) Triangular geogrid

Fig. 3 Single-sphere geogrid models: (a) square geogrid and (b) triangular geogrid with parallel bonds (black)

The system to generate the square geogrid in PFC3D is composed of basic square elements which create a simple junction with a rib in both longitudinal and transverse directions (represented by the red arrows in Fig. 4(a)). Meanwhile, the system to generate the triangular geogrid is composed of basic triangular elements which create a

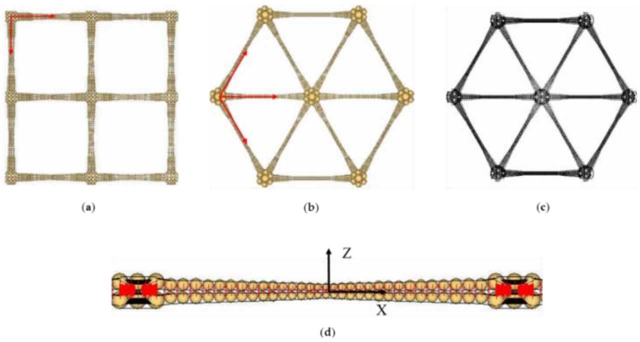

Fig. 4 Discrete element model of geogrids: (a) square geogrid with 9 nodes and 4 meshes, (b) triangular geogrid model, (c) parallel bond location of triangular geogrid and (d) side view between nodes

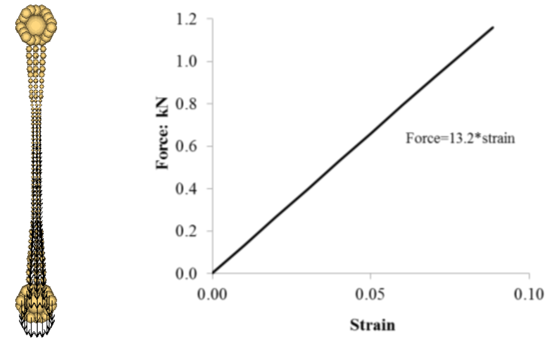

(a) Triangular geogrid rib model (b) Pullout force vs. strain

Fig. 5 Single rib test simulation

Table 2 Micromechanics parameters for triangular geogrid model

Parameters	Unit	Value
Parallel bond radius	mm	1.0
Parallel bond normal stiffness (LD)	N/m	4.03 e11
Parallel bond shear stiffness (LD)	N/m	5e5
Parallel bond normal strength (LD)	N	1.7e8
Parallel bond shear strength (LD)	N	1.4e7
Parallel bond normal stiffness (TD)	N/m	3.8e9
Parallel bond shear stiffness (TD)	N/m	5e5
Parallel bond normal strength (TD)	N	1.57e7
Parallel bond shear strength (TD)	N	1e7

* LD: longitude direction; TD: transverse direction

simple junction with a rib in all three directions, as shown in Fig. 4(b). Hence it follows that because of the high flexibility, this system can be used for setting up geogrids with different geometrical properties (e.g., aperture size) and for generating specific specimens which are required in calibration and following pull-out tests. The effect of shape of the geogrid on reinforced ballast performance in pullout test simulation would be compared.

Fig. 4(a) shows the new two-layer model for the square geogrid, comprising 816 small particles for each aperture. In contrast, Fig. 4(b) shows the new two-layer geogrid model for the triangular geogrid, comprising 929 small particles for each aperture, which means more contacts and more computational time. In addition, twenty-five particles have been added between at each junction of the triangular geogrid to support the rigidity under torsional loading. The model set-up was firstly performed by creating the nodes and then by adding the ribs between the nodes. The ribs comprise balls of different size, with smaller balls at the center of the ribs, to give the required geometry. A continuous slight decrease of the particle radii from the junction to the center of each rib is considered. Subsequently, all particles are bonded together by parallel bonds, which act over a circular cross-section between the two particles in contact and transmit both a force and a moment, as shown in Fig. 4(c). It should be noted that, because the bending resistances of ribs along the transverse and longitudinal directions are significantly different, the parallel bonds along the X and Y directions (black), as shown in Fig. 4(d), differ from the parallel bonds along the Z direction (red). The parameters will be calibrated in the following subsection.

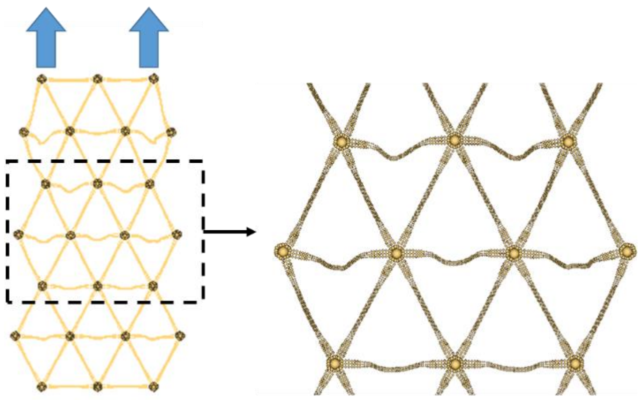

Fig. 6 The asymmetric buckling of triangular geogrid model under extension

3. Results and discussion

3.1 Calibration test

According to previous studies (Konietzky *et al*. 2004, Chen *et al*. 2012, 2014, Ngo *et al*. 2014), the parameters for the square geogrid were calibrated in terms of stiffness and strength by using a single rib extension test. The square geogrid model calibration was detailed in author's previous research (Chen *et al*. 2012). For the triangular geogrid model, the force at failure for a single rib extension test is 1.18 kN at a failure strain of 8.9%. Fig. 5 shows the rib tension test geometries and simulation results. The single rib extension test for the triangular geogrid was modelled using two nodes and a rib element. The upper nodes were fixed to simulate the junction clamp and a constant velocity was applied at the lower row of particles. The axial strain and the resulting forces at the lower rows of particles were monitored during the test. The parallel bond is depicted as a cylinder of elastic material in PFC3D. So the geogrid model has such a linear elastic-perfectly behavior. Experiments show some minor plastic deformation at larger strain but these are considered negligible for the purpose of these simulations.

For the calibration of the flexural rigidity of the geogrid, it has been well established that the buckling of columns is driven by the flexural rigidity of the member, which depends on the material properties and its geometrical properties, such as the second moment of area (moment of inertia) (I) (Gere and Goodno 2009). The second moment of area depends on the cross-sectional area shape. In this study, the cross-section two-layer rib consists of 2 × 3 spheres, as presented in Fig. 4. Fig. 6 shows the buckling of thirty apertures of a triangular geogrid pulled upwards simulated in DEM. The asymmetric buckling shown in the simulation is similar to the one observed experimentally. These results on the more complex triangular geogrid reinforce the indication that the mechanical behavior of geogrid can be reproduced by adequate arrangements of bonded spheres using bonds that can transmit forces and moments. The calibrated set of parameters as shown in Table 2 was used in the triangular geogrid simulations. These micromechanical parameters can be subdivided into deformation parameters (parallel bond stiffness) and strength parameters (parallel bond strengths). It seems that a better calibration of grid would not change the general behavior in terms of aggregate-grid interlock.

3.2 Interaction behavior between particle and geogrid

Pull-out tests are effective to investigate the mechanical interlock along the interface in geosynthetics reinforced zone. A series of large scale pull-out tests using different kinds of geogrid under different loading situations as shown in Fig. 7(a). The details of the experimental pull-out test are described in (Chen *et al*. 2014). Discrete element simulations of pullout test were also performed in order to reproduce the interlocking mechanism of geogrids from a micro point of view. It modelled pull-out tests with different load levels to investigate the interlocking behavior of geogrids under static loading conditions. Both the square geogrid and the soil particles were represented by particles using PFC3D. In conclusion, this micro scale numerical simulation approach is capable of modelling the most realistic interaction of ballast and geogrid by defining a properly properties of particles and geogrid, reproducing the actual geometry and accounting for the particle size distribution and shape.

Based on the geometrical properties of the selected square geogrid SSLA30, and triangular geogrid TX130, as described in Table 1, 11,657 particles are necessary to create one triangular geogrid sample with 20 triangular meshes, 4752 particles are necessary to create one square geogrid sample with nine meshes as shown in Figs. 7(b) and 7(c). In these simulations, a simplified-shape particle model was developed to represent ballast particles. This idealized-shape model is expected to offer an irregular shape using the least number of spheres necessary to provide particle interlock. The model chosen to meet these requirements simply consists of two overlapping spheres which total volume is identical to the average volume of the particles

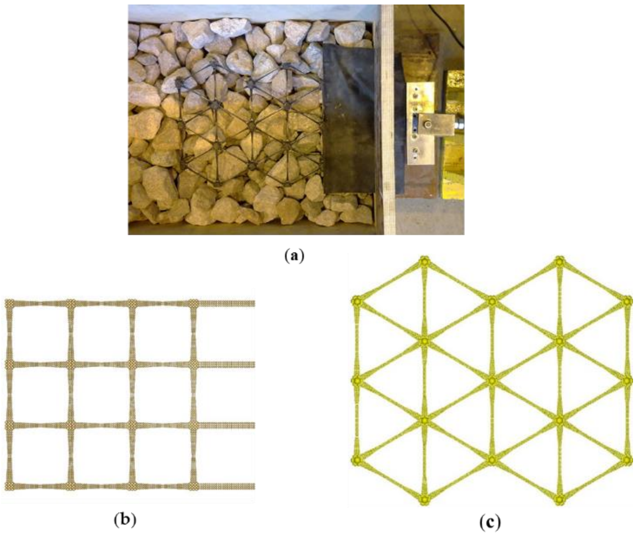

Fig. 7 Geogrid used in test and DEM: (a) laboratory pull out test triangular geogrid samplem (b) square geogrid model with 16 nodes and 9 apertures and (c) triangular geogrid with 17 nodes and 20 apertures

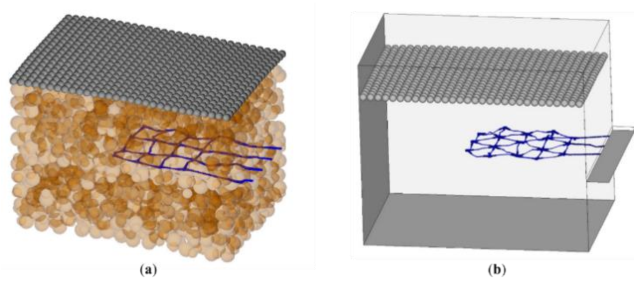

Fig. 8 PFC3D model for pull-out test simulations: (a) embedded with a square geogrid and (b) embedded with a triangular geogrid

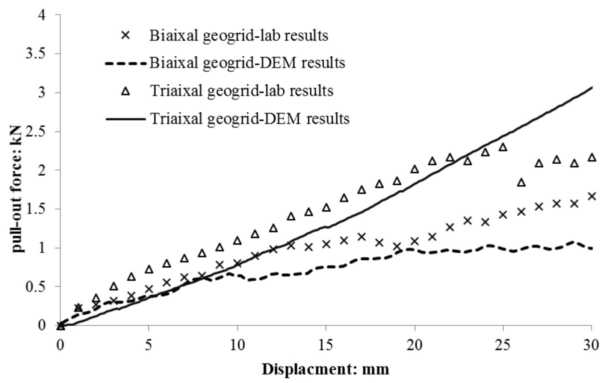

Fig. 9 Comparison of geogrid pullout resistance between experimental results and simulation results

(40 mm sphere) used in the realistic model. Fig. 8 shows the pullout test samples embedded with a square geogrid and a triangular geogrid. The top surcharge 0.5 kN was achieved by the self-weight of a plate-shaped clump. For these simulations, the normal and shear stiffness of the particles were 1.0×10^8 N/m and the stiffnesses of the walls were set to have the same values as the particles. The ball, box and geogrid friction coefficients were all set to be 0.6. The

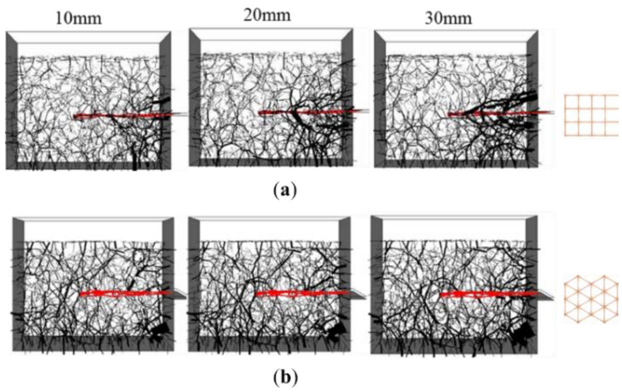

Fig. 10 Contact force network at different pulling distances: (a) square geogrids and (b) triangular geogrids

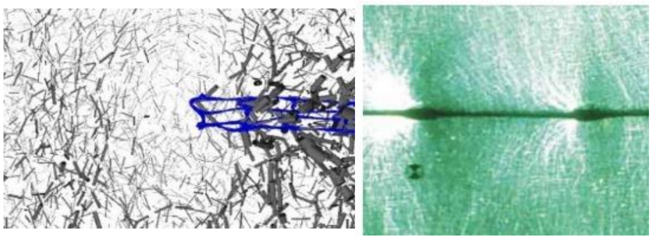

(a) 3D view of contact force from the transverse ribs (Chen 2009)

(b) "X-ray" test (Jenner *et al.* 2014)

Fig. 11 The interaction mechanism

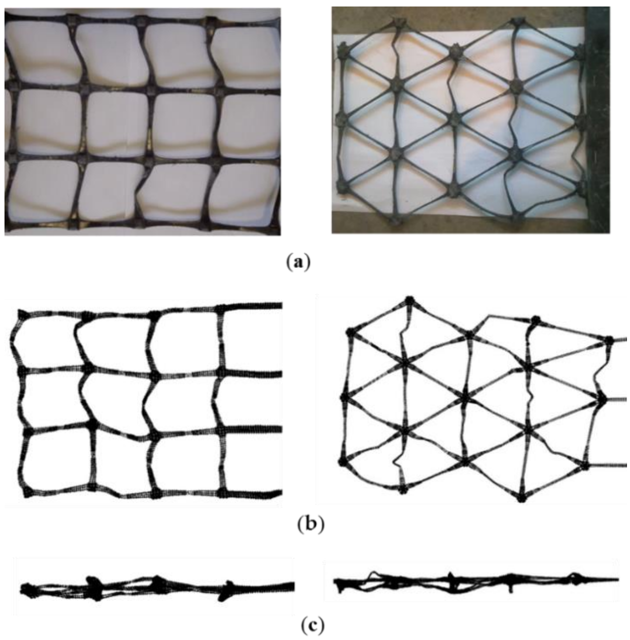

Fig. 12 Deformation behavior of square and triangular geogrid: (a) front view in experiments, (b) front view in DEM and (c) side view in DEM

density of the ballast particles was 2600 kg/m^3. A horizontal pull-out rate of 5 mm/s was given to the spheres at the right-hand end of the geogrid. To avoid any dynamic effects, the pull-out rate was gradually increased linearly with time from zero to the final rate after an initial 2 mm displacement.

Fig. 9 shows the development of the pullout force for the samples with different geogrid. Both the experimental and DEM results demonstrate that the triangular geogrid of aperture (rib) size 75 mm outperforms than square geogrid of aperture (rib) size 65 mm, by providing more pullout resistance, which is in agreement with the previous experimental and DEM cyclic loading test results (Chen *et al*. 2012, 2014). Moreover, it clearly indicates good agreement between DEM and experiments up to approximately 20 mm displacement although the DEM simulations have a little underestimate for the pullout force. It is believed that, owing to less angularity of the two-ball clumps, interlocking between the particle and geogrid is reduced compared to the real experiments comprising more angular particles. However, this paper is focus on the geogrid deformation behavior with different apertures. It seems that more complex shaped of particles would increase the computational time but not influence the comparison of the general interlocking behavior of geogrids.

Fig. 10 shows the comparison of the development of contact force distributions for several pullout stages between the square and triangular geogrids. It should be noted that contact forces are all drawn at the same scale. Fig. 10(a) displays the strong contact forces in the vicinity of the square geogrid area, which clearly shows the interlocking effect. This is in agreement with the simulation modelled by (McDowell *et al*. 2006). It also can be seen that, the clump ballast particles arch around each transverse rib during pull-out. Furthermore, the arching is concentrated on the back three transverse ribs after approximately 30 mm displacement, as shown in Fig. 10(a). The principal interlocking area has a range of about 10 cm thickness either sides of the square geogrid. For the sample with triangular geogrid, the contact force chains seem to be distributed evenly, which gives evidence of providing resistance at 3600. It should be note that a stress concentration is generated around the lower right corner during pullout as shown in Fig. 10(b). By comparison, it would be concluded that the triangular geogrid can reinforce the particles more effective than the square geogrid, and all the rib could provide the bearing resistance and spread the force in all directions.

It also can be seen from the 3D view that the clump ballast particles have arched around the transverse ribs during the pull-out, as shown in Fig. 11(a). Similarly, this is also observed in the special "X-ray" test (Fig. 11(b)), where the light areas represent zones of compression in front of the thick transverse ribs of the geogrid. It clearly shows that load is carried mainly by bearing on the thick transverse ribs, and transferred though the junctions to the longitudinal ribs at very small deformations (Jenner 2009).

3.3 Deformation behavior of square and triangular geogrid

The deformations of both square and triangular geogrids in the laboratory experiment and simulation are shown in Fig. 12, which clearly displays the extensive deformation of the geogrid, and deflection of the ribs can be seen in the side view. This deflection describes some of longitudinal ribs have negative strains, which are also observed in pull out test. Besides, the geogrid in the simulation seems to have more evident deformation compared with the experimental geogrid sample. This is because the geogrid deformation in the simulation was captured during the pull-out test, whereas it is not possible to view the whole deformed geogrid during the pull-out test in the laboratory, but only after the test when the geogrid has been removed.

4. Conclusions

The performed modelling of the two-layer realistic shaped geogrids including the square and triangular types have demonstrated that PFC3D is able to reproduce the deformation and strength characteristics of geogrids at least before reaching the maximum strength values (pre-failure-region). The main characteristics like the load-deformations behavior, the rotation rigidity, the tensile strength and shear strength of the square and triangular geogrid were reproduced by parallel bonds in PFC3D. The physics of the interlocking mechanism can be studied on a few meshes only in the pullout test simulations due to the limit of computational time. The simulation results have been shown to provide good predictions of pullout force as a function of displacement especially for the initial 30 mm displacement. Moreover, for the particle size of 40 mm, the triangular geogrid of aperture size 75 mm outperforms than the square geogrid of aperture size 65 mm, by providing more pullout resistance. Besides, the simulations have given valuable insight into the interaction between particle and geogrid and also revealed similar deformation behavior of the square and triangular geogrids during pullout. Therefore, the geogrid model allows a unique graphical demonstration of the interlocking mechanism which can be used to convince clients about the advantages and the physical behavior of a geogrid system. It will also enable the user to model other possible prototype geogrids using DEM, to investigate their performance before investing money in the manufacture of such geogrids.

Acknowledgments

The research described in this paper was financially supported by the National Natural Science Foundation of China (No. 51708438), the Fundamental Research Funds for the Central University (WUT: 2017 IVA 029; 2018 IVB029).

References

ASTM D6637. (2001), *Standard Test Method for Determining Tensile Properties of Geogrids by the Single or Multi-Rib Tensile Method*, American Society for Testing Materials, West Conshohocken, Pennsylvania, U.S.A.

Bhandari, A. and Han, J. (2010), "Investigation of geotextile-soil interaction under a cyclic vertical load using the discrete element method", *Geotext. Geomembranes*, **28**(1), 33-43.

Chen, C., McDowell, G.R. and Thom, N.H. (2012), "Discrete element modelling of cyclic loads of geogrid-reinforced ballast under confined and unconfined conditions", *Geotext. Geomembranes*, **35**, 76-86.

Chen, C., McDowell, G.R. and Thom, N.H., (2014), "Investigating geogrid-reinforced ballast: Experimental pull-out tests and discrete element modelling", *Soil. Found.*, **54**(1), 1-11.

Cundall, P.A. and Strack, O.D. (1979), "A discrete numerical model for granular assemblies", *Geotechnique*, **29**(1), 47-65.

Deb, K. and Konai, S. (2014), "Bearing capacity of geotextile-reinforced sand with varying fine fraction", *Geomech. Eng.*, **6**(1), 33-45.

Ferellec, J.F. and McDowell, G.R., (2012), "Modelling of ballast-geogrid interaction using the discrete-element method", *Geosynth. Int.*, **19**(6), 470-479.

Gere, J. and Goodno, B. (2004), *Stresses in Beams (Basic Topics)*, in *Mechanics of Materials*, Brooks/Cole Publishing Company, Belmont, California, U.S.A., 304-306.

Han, J. and Bhandari, A. (2011), "The influence of geogrid aperture size on the behavior of reinforced granular bases", *Proceedings of the International Symposiumon Geomechanics and Geotechnics: From Micro to Macro*, Shanghai, China, October.

Itasca (2008), *Particle Flow Code (PFC) in Three Dimension*, Itasca Consulting Group, Inc., Minneapolis, Minnesota, U.S.A.

Jenner, C. (2009), "Significant developments over the last 25 years", *Proceedings of the Jubilee Symposium on Polymer Geogrid Reinforcement*, London, U.K., September.

Kim, K.S., Yoon, Y.W. and Song, K.I. (2018), "Pullout resistance of treadmats for reinforced soil structures", *Geomech. Eng.*, **14**(1), 83-90.

Koerner, R.M. (2009), "An overview of geogrids", *Proceedings of the Jubilee Symposium on Polymer Geogrid Reinforcement*, London, U.K., September.

Konietzky, H., te Kamp, L. Groeger, T. and Jenner, C. (2004), "Use of DEM to model the interlocking effect of geogrids under static and cyclic loading", *Proceedings of the 2nd International PFC Symposium*, Kyoto, Japan, October.

Mahdi, M. and Katebi, H. (2015), "Numerical modeling of uplift resistance of buried pipelines in sand, reinforced with geogrid and innovative grid-anchor system", *Geomech. Eng.*, **9**(6), 757-774.

McDowell, G., Harireche, O., Konietzky, H., Brown, S. and Thom, N. (2006), "Discrete element modelling of geogrid-reinforced aggregates", *Proc. Inst. Civ. Eng. Geotech. Eng.*, **159**(1), 35-48.

Mulabdić, M. and Minažek, K. (2010), "Effect of transverse ribs of geogrids on pullout resistance", *Proceedings of the 9th International Conference on Geosynthetics*, Guarujá, Brazil, May.

Ngo, N.T., Indraratna, B. and Rujikiatkamjorn, C. (2014), "DEM simulation of the behavior of geogrid stabilised ballast fouled with coal", *Comput. Geotech.*, **55**, 224-231.

Qian, Y., Mishra, D., Tutumluer, E. and Kwon, J. (2013), "In comparative evaluation of different aperture geogrids for ballast reinforcement through triangular testing and discrete element modeling", *Proceedings of the 2013 Geosynthetics Conference*, Long Beach, California, U.S.A., April.

Stahl, M., Konietzky, H., Te Kamp, L. and Jas, H. (2014), "Discrete element simulation of geogrid-stabilised soil", *Acta Geotechnica*, **9**(6), 1073-1084.

Tensar International. (2010), *TriAx Brochure*, Tensar International Ltd, Blackburn, U.K.

Tutumluer, E., Huang, H. and Bian, X. (2010), "Geogrid-aggregate interlock mechanism investigated through aggregate imaging-based discrete element modeling approach", *Int. J. Geomech.*, **12**(4), 391-398.

Wang, Z., Jacobs, F. and Ziegler, M. (2014), "Visualization of load transfer behavior between geogrid and sand using PFC 2D",

Geotext. *Geomembranes*, **42**(2), 83-90.
Zhang, J., Yasufuku, N. and Ochiai, H. (2007), "A few considerations of pullout test characteristics of geogrid reinforced sand using DEM analysis", *Geosynth*. *Eng*. *J*., **22**, 103-110.

CC